JOURNAL OF AGRICULTURAL AND FOOD CHEMISTRY

Pseudoperoxidase Activity of Myoglobin: Kinetics and Mechanism of the Peroxidase Cycle of Myoglobin with H_2O_2 and 2,2-Azino-bis(3-ethylbenzthiazoline-6-sulfonate) as Substrates

CHARLOTTE U. CARLSEN,[†] IB M. SKOVGAARD,[‡] AND LEIF H. SKIBSTED*,[†]

Department of Dairy and Food Science, Food Chemistry, Royal Veterinary and Agricultural University, Rolighedsvej 30, DK-1958 Frederiksberg C, Denmark, and Department of Mathematics and Physics, Royal Veterinary and Agricultural University, Thorvaldsensvej 40, DK-1871 Frederiksberg C, Denmark

Using 2,2-azino-bis(3-ethylbenzthiazoline-6-sulfonate) (ABTS) as substrate, it has been shown that the increased peroxidase activity for decreasing pH of myoglobin activated by hydrogen peroxide is due to a protonization of ferrylmyoglobin, MbFe(IV)═O, facilitating electron transfer from the substrate and corresponding to p$K_a \sim 5.2$ at 25.0 °C and ionic strength 0.16, rather than due to specific acid catalysis. On the basis of stopped flow absorption spectroscopy with detection of the radical cation $ABTS^{\bullet+}$, the second-order rate constant and activation parameters for the reaction between MbFe(IV)═O and ABTS were found to have the values $k = 698 \pm 32$ M^{-1} s^{-1}, $\Delta H^{\#} = 66 \pm 4$ kJ mol^{-1}, and $\Delta S^{\#} = 30 \pm 15$ J mol^{-1} K^{-1} at 25.0 °C and physiological pH (7.4) and ionic strength (= 0.16 M NaCl). At a lower pH (5.8) corresponding to the conditions in meat, values were found as follows: $k = 3.5 \pm 0.3 \times 10^4$ M^{-1} s^{-1}, $\Delta H^{\#} = 31 \pm 6$ kJ mol^{-1}, and $\Delta S^{\#} = -53 \pm 19$ J mol^{-1} K^{-1}, indicative of a shift from outersphere electron transfer to an innersphere mechanism. For steady state assay conditions, this shift is paralleled by a shift from saturation kinetics at pH 7.4 to first-order kinetics for H_2O_2 as substrate at pH 5.8. In contrast, the activation reaction between myoglobin and hydrogen peroxide was found at 25.0 °C to be slow and independent of pH with values of 171 ± 7 and 196 ± 19 M^{-1} s^{-1} found at physiological and meat pH, respectively, as determined by sequential stopped flow spectroscopy, from which a lower limit of $k = 6 \times 10^5$ M^{-1} s^{-1} for the reaction between perferrylmyoglobin, •MbFe(IV)═O, and ABTS could be estimated. As compared to the traditional peroxidase assay, a better characterization of pseudoperoxidase activity of heme pigments and their denatured or proteolyzed forms is thus becoming possible, and specific kinetic effects on activation, substrate oxidation, or shift in rate determining steps may be detected.

KEYWORDS: Transient state kinetics; myoglobin; ABTS; hydrogen peroxide; pseudoperoxidase activity

INTRODUCTION

Myoglobin possesses peroxidase-like activity and catalyzes the oxidation of various compounds following the reaction with hydrogen peroxide. However, as elucidated from mechanistic studies with various myoglobin mutants (*1*−*3*), differences in heme packing between myoglobin and native peroxidases result in lower catalytic activity of the myoglobin peroxidase cycle as compared to the cycle of real peroxidases (*4*).

The lower catalytic activity of myoglobin is counteracted by a higher concentration of myoglobin in muscles, and the hypervalent forms of myoglobin [perferrylmyoglobin (•MbFe(IV)═O) and ferrylmyoglobin (MbFe(IV)═O)] formed during the (pseudo)peroxidase cycle have accordingly received increasing attention due to a possible influence on oxidation in biological tissue and in meat systems. Both •MbFe(IV)═O and MbFe(IV)═O are deactivated either in so-called autoreductions during which the proteins are modified (*5*, *6*) or in the presence of reducing agents (*7*−*9*), the nature of which determines the overall effect of the pseudoperoxidase cycle. Water soluble antioxidants such as ascorbate and chlorogenate (*8*) will be oxidized to rather stable antioxidant radicals, while an oxidation of, e.g., lipid hydroperoxides (*10*) or nitrite (*9*) may be more harmful since the oxidation products may propagate oxidation reactions. Also, a further consequence of oxidative processes of long-lived protein radicals formed by oxidation of proteins

* To whom correspondence should be addressed. Tel: +4535283221. Fax: +4535283344. E-mail: ls@kvl.dk.
[†] Department of Dairy and Food Science, Food Chemistry, Royal Veterinary and Agricultural University.
[‡] Department of Mathematics and Physics, Royal Veterinary and Agricultural University.

10.1021/jf030067g CCC: $25.00
Published on Web 08/14/2003

by hydrogen peroxide-activated myoglobin is a matter of discussion (*11*). Most studies of hypervalent myoglobins are performed at neutral pH to assemble the situation in living tissue. However, for myoglobin in the digestive tract with local pH gradients and for meat systems with the characteristic postmortem pH decrease, the pH dependence of the pseudoperoxidase activity of myoglobin becomes important, since the reactivity of MbFe(VI)═O clearly increases when pH decreases (*6*, *8*). In addition to an effect of a pH decrease, other factors such as proteolysis, changes in ionic strength, and protein cross-linkings should be further explored for a possible enhancement of the pseudoperoxidase activity of myoglobin. Such enhancements are clearly of importance when evaluating the significance of myoglobins peroxidase activity, and it is our attempt to find a suitable system to model kinetically the pseudoperoxidase activity of myoglobin including that of partly modified myoglobin molecules. We have chosen the well-known peroxidase substrate 2,2-azino-bis(3-ethylbenzthiazoline-6-sulfonate) (ABTS), since its oxidized form, $ABTS^{\bullet+}$, has a significant absorption in the near-infrared region, where the absorption of heme pigments are negligible, and we have exploited the stopped flow technique to generate and follow the reactions of the transient states of myoglobin.

MATERIALS AND METHODS

Chemicals. Metmyoglobin (MbFe(III), horse heart, type III), ABTS, 2-[*N*-morpholino]ethansulfonic acid (MES), and bovine liver catalase (51 000 units/mg protein, 47.4 mg protein/ml) were obtained from Sigma Chemical Co. (St. Louis, MO). Analytical grade hydrogenperoxide (H_2O_2) was from Riedle-de-Haën (Selze, Germany). HCl (0.2000 M) was purchased from Bie & Berntsen Laboratory (Bie & Berntsen A/S, Rødovre, Denmark). All other chemicals (analytical grade) were from Merck (Darmstadt, Germany). Water was purified through a Millipore Q-Plus purification train (Millipore Corp., Bedford, MA).

pH Measurements. The pH_a ($pH_a = -\log a_{H^+}$) of solutions and samples was measured by a Me6.0224.100 combination glass microelectrode connected to a Methrom 713 pH meter (Methrom, Herisau, Switzerland) standardized to the international pH standards. In addition, for use in calculations of kinetic constants, pH_c in reaction samples was measured relative to concentration standards (0.0100 M HCl and 0.00100 M HCl, ionic strength 0.16 adjusted with NaCl), using the same electrode and employing the definition $pH = -\log[H^+]$. Unless otherwise stated in the text by a pH_c, all given pH values are pH_a values.

Purification of MbFe(III) and Synthesis of MbFe(IV)═O. MbFe(III) dissolved in 5.0 M phosphate buffer (ionic strength 0.16, adjusted with NaCl) was purified on a Shephadex G25 column (40 cm × 2.5 cm, Pharmacia Biotech AB, Uppsala, Sweden). The eluted MbFe(III) was diluted with the phosphate buffer to yield the desired concentrations as determined spectrophotometrically at 525 nm, $\epsilon_{525\ nm} = 7700\ M^{-1}\ cm^{-1}$ (*12*). For experiments with MbFe(IV)═O, the purified MbFe(III) was reacted with H_2O_2 (ratio 1:3) for 3.0 min. The reaction was stopped by adding 10 μL of catalase, and the identity of the formed MbFe(IV)═O was confirmed by absorption spectroscopy (*13*). In addition, from the obtained absorbance spectrum, the MbFe(IV)═O concentration was calculated according to the following equation (*14*):

$$[\text{MbFe(IV)═O}]\ (\mu M) = -62\,(A_{490nm} - A_{700nm}) + 242\,(A_{650nm} - A_{700nm}) - 123\,(A_{580nm} - A_{700nm}) \quad (1)$$

To avoid significant decay of MbFe(IV)═O before kinetic experiments, only small volumes of MbFe(IV)═O solutions were synthesized at a time as required for one series of stopped flow experiments. H_2O_2 concentrations were determined spectrophotometrically, $\epsilon_{240nm} = 39.4\ M^{-1}\ cm^{-1}$ (*15*).

Transient State Kinetic Experiments. From stock solutions of ABTS (0.35 mM), buffered ABTS solutions were made shortly before use by appropriate dilution with MES or phosphate buffer solutions and adjustment to a final ionic strength of 0.16 with NaCl. ABTS stock solutions were used within 5 days during which period of time, no degradation could be detected spectrophotometrically ($\epsilon_{340nm} = 3.6 \times 10^4\ M^{-1}\ cm^{-1}$ (*16*)) in solutions protected against light.

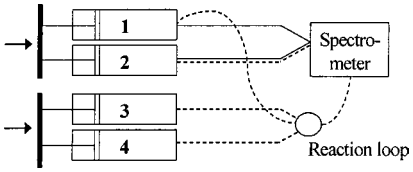

Figure 1. Shematics of the regular and sequential mixing modes of stopped flow spectroscopy as used to study the reaction between ABTS and •MbFe(IV)═O or MbFe(IV)═O. Straight lines, regular mixing mode as used for MbFe(IV)═O; dotted lines, sequential mixing mode as used for •MbFe(IV)═O. The syringes are numbered 1–4.

For the kinetic experiments with MbFe(IV)═O, MbFe(IV)═O solution and ABTS solution were placed in each syringe of a DX-17MV stopped flow spectrofluorometer in its regular mixing mode (Applied Photophysics, London, U.K.), and the reactions were followed by absorbance measurements at 734 nm ($\epsilon_{ABTS^{\bullet+},734nm} = 1.5 \times 10^4\ M^{-1}\ cm^{-1}$ (*17*)). Initial reaction rates and pseudo-first-order rate constants were calculated by linear and nonlinear regression analysis, using the SX.18 MV software connected to the stopped flow spectrometer (Applied Photophysics). In the kinetic experiments, MbFe(IV)═O was in excess relative to ABTS by at least a factor of 10, the buffer concentration was 30 mM, and the ionic strength was 0.16 ± 0.01 adjusted with NaCl. Two parts of the final experiment, where initial reaction rates were calculated, had a preset value of pH of 5.8 and 7.4, and of these, 3−14 regular mix stopped flow experiments were made for each combinations of temperatures (9, 13, 19, or 25 °C at pH 5.8 and 14, 19, or 25 °C at pH 7.4) and four concentrations of MbFe(IV)═O. In a third part of the final experiment, temperature and concentration of MbFe(IV)═O were held constant while the pH was set at six different values between 5.39 and 7.35. In this series, between 9 and 13 stopped flow experiments were made for each combination. For each set of experimental conditions, pH_c and pH_a were measured in thermostated 1:1 mixtures of the MbFe(IV)═O and ABTS solutions.

In kinetic experiments with •MbFe(IV)═O, the sequential mixing mode of the stopped flow spectrometer was used (see **Figure 1**). The syringes nos. 3 and 4 contained MbFe(III) and H_2O_2 in 5.0 mM phosphate buffer. The contents of these syringes were mixed in a thermostated loop, and after varying aging times, the loop solution was mixed with ABTS solution from syringe no. 2. Syringe no. 1 contained buffer ($I = 0.16$) for flushing. The reaction was followed by absorbance measurements at 734 nm, the buffer concentration was 30 mM, and the ionic strength was 0.16 (NaCl). In the reaction mixture, H_2O_2 and myoglobin were in excess relative to ABTS by a factor of at least 50 (as determined from initial concentrations of MbFe(III) and H_2O_2), and in the thermostated loop, the concentration of H_2O_2 was always 1.5−2.4 times the concentration of MbFe(III). Sixteen combinations of H_2O_2 concentration, MbFe(III) concentration, and pH resulted in 105 individual sequential stopped flow experiments, and for each set of conditions, pH_a and pH_c were measured in thermostated 1:1/2:1/2 mixtures of the ABTS, MbFe(III), and H_2O_2 solutions.

Steady State Kinetic Experiments. The activity for one electron oxidation of ABTS at pH 7.4 or 5.8 was measured for MbFe(III) in the presence of H_2O_2 at 25.0 °C as rate of formation of $ABTS^{\bullet+}$ by the use of an HP8453 UV−vis diode array spectrophotometer. Formation of the $ABTS^{\bullet+}$ radical was followed by absorbance readings between 400 and 800 nm with time intervals of 8 s, and values for $[ABTS^{\bullet+}]/t$ were determined from the increase in absorbance vs time at 734 nm ($\epsilon_{ABTS^{\bullet+},734nm} = 1.5 \times 10^4\ M^{-1}\ cm^{-1}$ (*17*)). The final reaction volumes were 2.00 mL and contained 0.50 μM MbFe(III), 1.0 mM ABTS, and variable $[H_2O_2]$ (0.025−0.850 mM) in aqueous 50 mM MES or phosophate buffer. pH_a and pH_c were measured in the reaction mixtures after the recording of the absorption spectra was finished.

Fitting of Kinetic Models to Experimental Data. Kinetic models were fitted to the experimental data by means of linear or nonlinear

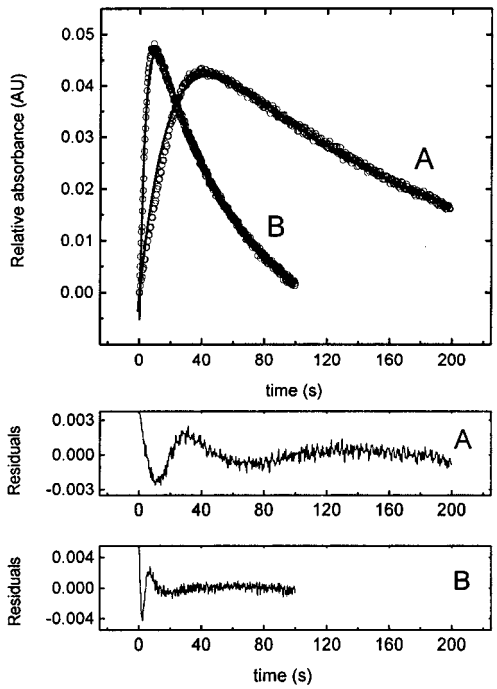

Figure 2. Relative absorbance at 734 nm during the reaction between MbFe(IV)═O and ABTS. (**A**) At 10.7 °C, reaction between 223.0 μM MbFe(IV)═O and 5.6 μM ABTS [0.02 mM phosphate buffer, pH 7.35, I = 0.16 (NaCl)]. (**B**) At 25.3 °C, reaction between 220.1 μM MbFe(IV)═O and 5.6 μM ABTS [0.02 mM phosphate buffer, pH 7.36, I = 0.16 (NaCl)]. Experimental points (circles) overlap fitted lines (straigth lines). Lower panels show residuals from nonlinear regression analysis: $A_{734\text{nm},t} = \alpha \exp(-k_{1\text{conseq}}t) + \beta \exp(-k_{2\text{conseq}}t) + A_{734\text{nm},\infty}$, from which the pseudo-first-order rate constants were obtained as follows: $k_{1\text{conseq}} = 4.96 \times 10^{-2} \pm 0.12 \times 10^{-2}$ s^{-1} and $k_{2\text{conseq}} = 8.84 \times 10^{-3} \pm 0.56 \times 10^{-3}$ s^{-1} (**A**) and $k_{1\text{conseq}} = 0.287 \pm 0.004$ s^{-1} and $k_{2\text{conseq}} = 1.91 \times 10^{-2} \pm 0.04 \times 10^{-2}$ s^{-1} (**B**).

regression using the SAS system (8.2, SAS Institute, Inc., Cary, NC). In all parts of the analysis, standard errors of the estimated constants were obtained by standard methods from the linear or nonlinear regression analysis, and models were checked by comparing data with fitted values graphically and by plotting residuals against fitted values, concentration, pH, and temperature.

RESULTS

MbFe(IV)═O and •MbFe(IV)═O were both generated by reaction with H_2O_2, and both were found to be reduced by ABTS in aqueous solution. However, two different techniques had to be used to study the kinetics of their reduction, since the half-life of autoreduction of MbFe(IV)═O (~20 min at ambient temperature at pH of meat and slower at neutral pH (*6*)) is clearly different from the half-life of autoreduction of •MbFe(IV)═O (7−30 s at neutral pH (*5*)).

Regular stopped flow absorption spectroscopy was used to follow the reaction between MbFe(IV)═O and ABTS using a large excess of MbFe(IV)═O relative to ABTS. As seen in **Figure 2**, this resulted in pseudo-first-order formation and decay of the green radical $ABTS^{\bullet+}$, which absorbs strongly at 734 nm. MbFe(IV)═O was in excess relative to ABTS allowing two one electron transfers to take place

$$\text{ABTS} \rightarrow \text{ABTS}^{\bullet+} + e^- \rightarrow \text{ABTS}^{2+} + e^- \qquad (1)$$

resulting in the colorless $ABTS^{2+}$ cation as the end product. Rate constants for this consequtive reaction were calculated by

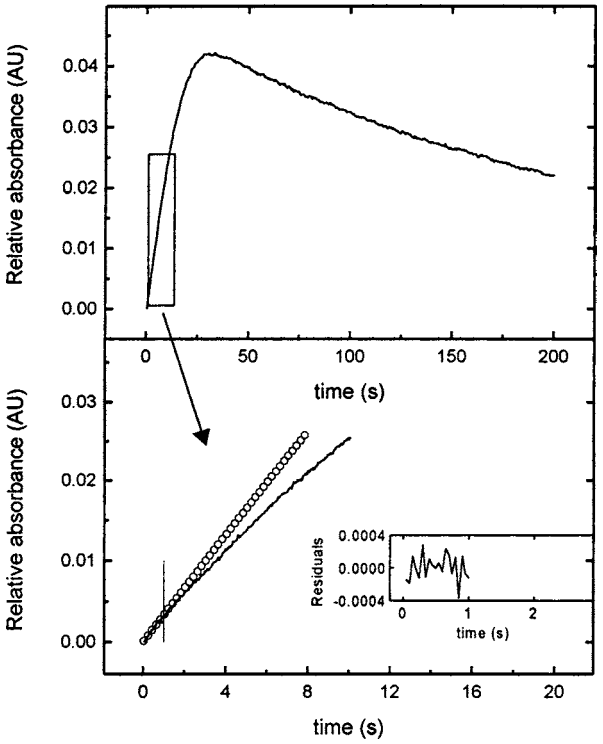

Figure 3. Initial reaction profile at 734 nm during the reaction at 25.0 °C between 55.5 μM MbFe(IV)═O and 5.5 μM ABTS [30 mM phosphate buffer, pH 7.42, I = 0.16 (NaCl)]. Upper panel: Relative absorbance at 734 nm during the reaction at full time scale. Lower panel: Relative absorbance at 734 nm during the initial part of the reaction together with residuals from a linear fit to the absorbance changes during the first second of reaction from which a value of $k_{\text{obs}} = 3.28 \times 10^{-3} \pm 0.12 \times 10^{-3}$ M^{-1} s^{-1} was calculated.

nonlinear regression of the expression

$$A_{734\text{nm},t} = \alpha \exp(-k_{1\text{conseq}}t) + \beta \exp(-k_{2\text{conseq}}t) + A_{734\text{nm},\infty} \qquad (2)$$

to the absorbance data (see **Figure 2**). α and β are constants relating to the absorptivities of the reactant, intermediate, and product, and $k_{1\text{conseq}}$ and $k_{2\text{conseq}}$ are (pseudo)first-order rate constants for the formation and decay of the intermediate $ABTS^{\bullet+}$. Reaction times and the rate constants calculated from **Figure 2** show a significant temperature dependence of the reaction, and a clear dependence on MbFe(IV)═O concentration and on pH was also observed for the rate constants obtained in similar kinetic experiments (data not shown). However, as compared to the difference in reaction rates obtained varying the reaction conditions (MbFe(IV)═O concentration, pH, and temperature), the standard deviations of rate constants from repetitive experiments (calculated by means of eq 2) were too high to allow a detailed kinetic analysis of the two steps in the consecutive reactions. Instead, initial reaction rates were used in kinetic analysis of the first reaction (see **Figure 3**), and thus, only the kinetics of formation of $ABTS^{\bullet+}$, but not the kinetics of the decay of $ABTS^{\bullet+}$, was further investigated. For the reaction conditions used, the reaction is assumed to be of second-order, and the rate of formation of $ABTS^{\bullet+}$ depends on ABTS and MbFe(IV)═O concentrations according to

$$\frac{\text{d}[\text{ABTS}^{\bullet+}]}{\text{d}t} = k_2\,[\text{ABTS}]\,[\text{MbFe(IV)═O}] \qquad (3)$$

The slope of the initial part of the reaction profiles ($\text{d}A_{734\text{nm}}/\text{d}t$)

Table 1. Rate Constants (25.0 °C) and Activation Parameters at pH 5.8 and pH 7.4 in Aqueous Solution with Ionic Strength 0.16 for the Reactions in the Pseudoperoxidase Cycle of Myoglobin Driven with Hydrogen Peroxide and ABTS as Substrates; Results Are Given as Estimates ± Standard Error

	pH 5.8[a]			pH 7.4[b]		
	k (M^{-1} s^{-1})	$\Delta H^{\#}$ (kJ mol^{-1})	$\Delta S^{\#}$ (J mol^{-1} K^{-1})	k (M^{-1} s^{-1})	$\Delta H^{\#}$ (kJ mol^{-1})	$\Delta S^{\#}$ (J mol^{-1} K^{-1})
MbFe(III) + H_2O_2	196 ± 19			171 ± 7		
•MbFe(IV)═O + ABTS	>6 × 10^5			>6 × 10^5		
MbFe(IV)═O + ABTS	3.5 × 10^4 ± 0.3•10^4[c]	31 ± 6	−53 ± 19	698 ± 32[c]	66 ± 4	30 ± 15

[a] For the reaction of ABTS with mixtures of MbFe(III) + H_2O_2 to yield •MbFe(IV)═O, all experiments are carried out at pH 5.74, and for the reaction between MbFe(IV)═O + ABTS, the experiments are carried out at pH 5.76–5.85. [b] For the reaction of ABTS with mixtures of MbFe(III) + H_2O_2 to yield •MbFe(IV)═O, all experiments are carried out at pH 7.40, and for the reaction MbFe(IV)═O + ABTS, the experiments are carried out at pH 7.35–7.42. [c] Estimated from $\Delta H^{\#}$ and $\Delta S^{\#}$ using the transition state theory.

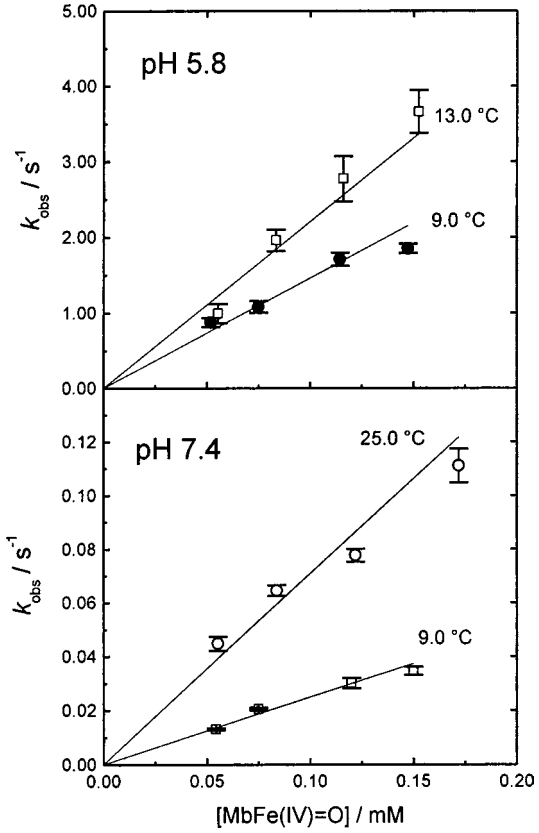

Figure 4. Observed first-order rate constants obtained as shown in **Figure 3** as a function of MbFe(IV)═O concentration for the reaction between MbFe(IV)═O and ABTS at an excess concentration of MbFe(IV)═O and ionic strength 0.16 (NaCl). Experimental points are compared with the lines as calculated according to eq 5.

was used to calculate an observed rate constant, k_{obs}:

$$k_{obs} = \frac{d[ABTS^{\bullet+}]}{dt\,[ABTS]} = \frac{dA_{734nm}}{dt\,\epsilon_{ABTS,734nm}\,l\,[ABTS]} \qquad (4)$$

which accordingly should depend linearly on the MbFe(IV)═O concentration:

$$k_{obs} = k_2\,[MbFe(IV)═O] \qquad (5)$$

By varying the concentration of MbFe(IV)═O, concentration profiles at different temperatures were obtained at two selected pH values: ∼7.4 as a representative of the living muscle and ∼5.8 as a representative of meat. Four concentration profiles are included in **Figure 4**, and as may be seen, reaction rates are higher at the pH of meat as compared to the living muscle.

In addition, **Figure 4** shows that k_{obs} increases with increasing MbFe(IV)═O concentrations and with increasing temperature, and the linear dependence of k_{obs} on [MbFe(IV)═O] confirms the assumption of a second-order reaction of eq 3. By including different temperatures in the investigation, an estimation of activation parameters from k_{obs} for the reaction between ABTS and MbFe(IV)═O (at pH 5.8 and 7.4) became possible by using transition state theory:

$$\frac{k_{obs}}{[MbFe(IV)═O]} = \frac{k_B T}{h}\exp\left(\frac{\Delta S^{\#}}{R}\right)\exp\left(\frac{-\Delta H^{\#}}{RT}\right) \qquad (6)$$

For each of the two pH values, 5.8 and 7.4, the model in eq 6 was fitted to the data given by the measured value of k_{obs} using the method of least squares. To obtain homogeneous error variance, the data had first to be logarithmically transformed, however, so that ln(k_{obs}) was modeled by the logarithm of the right-hand side of eq 6. Furthermore, because observations within groups defined by the same value of temperature and concentration of MbFe(IV)═O were evidently correlated, the average value of ln(k_{obs}) was used as the response variable, thus fitting the eq 6 to 16 and 12 data points for pH 5.8 and pH 7.4, respectively. Computationally, the fitting was done by a linear regression analysis, subtracting the known terms on the right-hand side of eq 6 from the values of ln(k_{obs}) and regressing on the inverse temperature to estimate the two unknown constants $\Delta S^{\#}$ and $\Delta H^{\#}$ for each of the two selected values of pH. The estimated activation parameters for the reactions are given in **Table 1**. **Figure 5** shows the temperature dependence of the reaction at the two pH values investigated as an Arrhenius type plot for k_2.

To support the results obtained at the two selected pH values, the pH dependence of the reaction was investigated for a fixed temperature and MbFe(IV)═O concentration. The obtained pH profile is shown in **Figure 6**, where k_{obs} is seen to increase as pH decreases. This pH_c dependence of the reduction of MbFe(IV)═O is in agreement with an earlier described reaction model including an acid base equilibrium of MbFe(IV)═O:

$$k_{obs} = k_a\,[MbFe(IV)═O,H^+] + k_b\,[MbFe(IV)═O] = \left(k_a\frac{[H^+]}{[H^+]+K_a} + k_b\frac{K_a}{[H^+]+K_a}\right)C^{total}_{MbFe(IV)═O} \qquad (7)$$

where K_a is the acid dissociation constant for the protonated form of ferrylmyoglobin (MbFe(IV)═O,H^+) and k_a and k_b are the rate constants for the reduction of the protonated and nonprotonated form of MbFe(IV)═O. The logarithmically transformed version of eq 7 was fitted using nonlinear regression to the data in **Figure 6**, using averages of ln(k_{obs}) within groups given by the same pH. This resulted in a pK_c value of 5.22 ±

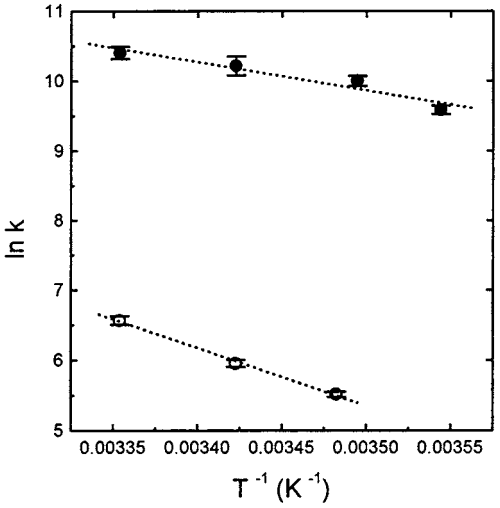

Figure 5. Arrhenius type plot for the second-order rate constant for reaction between MbFe(IV)=O and ABTS, determined at pH 7.4 and pH 5.8 at ionic strength 0.16 (NaCl). Data points are ln-transformed values of $k_2 \pm$ standard error obtained by linear regression of the data at each temperature; cf. **Figure 4**. Dotted lines are obtained from the activation parameters (**Table 1**) obtained when the temperature is directly included in the numerical analysis according to eq 6.

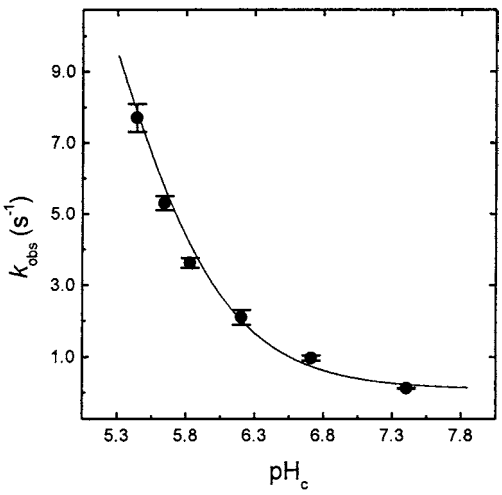

Figure 6. Dependence of k_{obs}, obtained from initial rates as shown in **Figure 3**, on pH_c for the reaction between 97.8 ± 6.5 μM MbFe(IV)=O and 5.5 μM ABTS at 25.0 °C in aqueous solutions of ionic strength 0.16 (NaCl). Average data points (±SD) are compared with a curve as estimated by nonlinear regression of eq 7 to the experimental rate constants, giving a pK_a value of 5.22 ± 0.39 for the acid–base equilibrium of ferrylmyoglobin.

0.39 at 25.0 °C for the acid−base equilibrium between the protonated and the nonprotonated MbFe(IV)=O, a value similar to values obtained in other studies for reduction of MbFe(IV)=O by other reductants (*6*, *8*).

The kinetics of reduction of •MbFe(IV)=O by ABTS was studied by sequential stopped flow absorption spectroscopy. Typical reaction profiles are shown in **Figure 7** for experiments with different aging times, and as may be seen from the figure, the reaction rate and reaction order change as the mixed MbFe(III) and H_2O_2 solutions are aged before reaction with ABTS. At long aging times, the formed •MbFe(IV)=O autoreduces to MbFe(IV)=O before the mixing with ABTS takes place, and the reaction becomes of pseudo-first-order as was the case in the regular stopped flow experiments; see **Figure 2**. However, at short aging times, •MbFe(IV)=O will not have time to decay

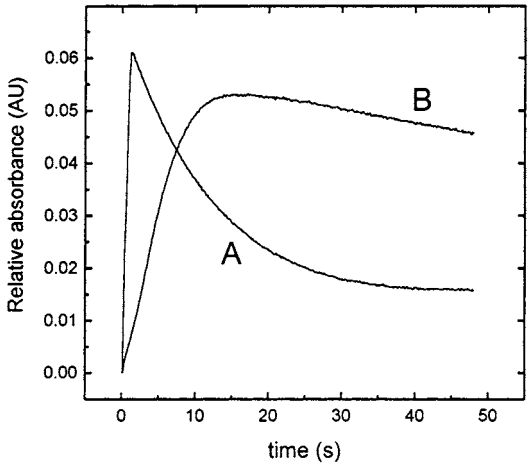

Figure 7. Relative absorbance at 734 nm during reaction between H_2O_2-activated MbFe(III) and ABTS at pH 7.40 (20 mM phosphate buffer), 25.0 °C, and $I = 0.16$ (NaCl). By use of sequential stopped flow absorption spectroscopy (cf. **Figure 1**), two different aging times for the reaction between 750 μM H_2O_2 and 504 μM MbFe(III) are used (**A**, 0.029 s; **B**, 200 s), before exposure to 5.6 μM ABTS.

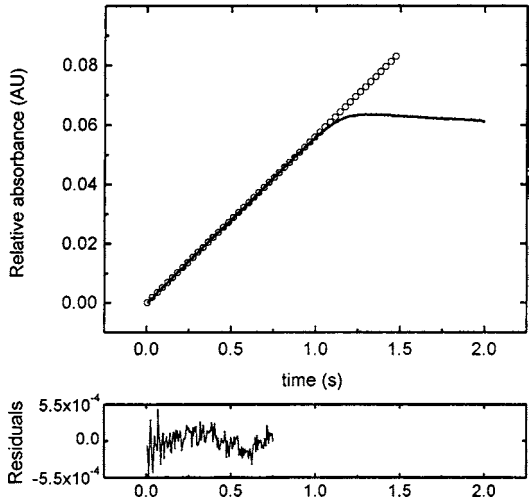

Figure 8. Reaction profile at 734 nm during the reaction between H_2O_2-activated MbFe(III) and ABTS at 25.0 °C and pH 7.40. H_2O_2 (750 μM) and MbFe(III) (504 μM) were aged for 29 ms before mixing with 5.6 μM ABTS. The lower panel shows residuals from a linear fit to the first part of the profile from which an apparent zero-order rate constant, $k_{zero} = 5.63 \times 10^{-2} \pm 0.01 \times 10^{-2}$, was obtained.

before the reaction with ABTS takes place, and the reaction profile now seems to be of zeroth order. For intermediate aging times, a mixed reaction order was observed.

As illustrated in **Figure 8**, zeroth order rate constants, k_{zero}, could be calculated by linear regression of the reaction profiles obtained at the short aging time for different combinations of H_2O_2 and MbFe(III) concentrations at pH 5.8 and 7.4.

A zero-order reaction as described above was earlier observed in a study of reduction of •MbFe(IV)=O by the water soluble carotenoid crocin (*7*), and as for this reaction, a zero-order reaction rate for the reaction between •MbFe(IV)=O and ABTS is in agreement with the following analogous reaction sequence:

$$\text{MbFe(III)} + H_2O_2 \rightarrow \bullet\text{MbFe(IV)=O} + H_2O \quad (8)$$

$$\bullet\text{MbFe(IV)=O} + \text{ABTS} \rightarrow \text{MbFe(IV)=O} + \text{ABTS}^{\bullet+} \quad (9)$$

$$\text{MbFe(IV)=O} + \text{ABTS} \rightarrow \text{MbFe(III)} + \text{ABTS}^{\bullet+} \quad (10)$$

provided that the reaction of eq 8 is rate determining, with the reaction of eq 9 very much faster than the reaction of eq 8 ($k_9 \gg k_8$) and with the reaction of eq 10 being negligible at short aging times. •MbFe(IV)═O will be present in a steady state concentration under these conditions:

$$\frac{d[\bullet MbFe(IV)=O]}{dt} = k_8 [H_2O_2] [MbFe(III)] - k_9 [\bullet MbFe(IV)=O] [ABTS] = 0 \quad (11)$$

Because the formation of $ABTS^{\bullet+}$ in this case (short aging times) is dominated by the reaction with •MbFe(IV)═O (eq 9) and not with MbFe(IV)═O (eq 10), the rate of formation of $ABTS^{\bullet+}$:

$$\frac{d[ABTS^{\bullet+}]}{dt} = k_9 [\bullet MbFe(IV)=O] [ABTS] + k_{10} [MbFe(IV)=O] [ABTS] \approx k_9 [\bullet MbFe(IV)=O] [ABTS] \quad (12)$$

can be expressed as:

$$\frac{d[ABTS^{\bullet+}]}{dt} = k_8 [H_2O_2] [MbFe(III)] \quad (13)$$

from which zeroth order kinetics for formation of $ABTS^{\bullet+}$ is expected for conditions of excess H_2O_2 and of excess MbFe(III). By integration of eq 13, the actual concentration of $ABTS^{\bullet+}$ at a given time is expressed as

$$[ABTS^{\bullet+}]_t = [ABTS^{\bullet+}]_0 + k_8 [H_2O_2] [MbFe(III)] t \quad (14)$$

and substituting this expression into the relation between absorbance at 734 nm (where $ABTS^{\bullet+}$ absorbance dominates) and $ABTS^{\bullet+}$ concentration

$$A_{t(734nm)} = A_{0(734nm)} \frac{[ABTS^{\bullet+}]_t}{[ABTS^{\bullet+}]_0} \quad (15)$$

the following equation is obtained

$$A_{t(734nm)} = A_{0(734nm)} + \frac{k_8 [H_2O_2] [MbFe(III)] A_{0(734nm)}}{[ABTS^{\bullet+}]_0} t \quad (16)$$

Accordingly, the rate constant k_8 for the rate-determining reaction of eq 8 can be calculated from the slope (α) of a linear plot of the observed zeroth order rate constant (k_{zero}, obtained as shown in **Figure 8**) as a function of varying H_2O_2 at constant concentration of MbFe(III) or as a function of varying MbFe(III) at constant concentration of H_2O_2 ($\alpha = k_{zero}/[H_2O_2]$ or $\alpha = k_{zero}/[MbFe(III)]$):

$$k_8 = \frac{k_{zero}}{l \epsilon_{734nm} [H_2O_2] [MbFe(III)]} \quad (17)$$

where $A_{0(734nm)}/[ABTS^{\bullet+}]$ is further substituted with $l \epsilon_{734nm}$, the product of the optical path length of the spectrophotometer and the molar absorptivity of $ABTS^{\bullet+}$. **Figure 9** shows such linear plots for the two pH values 5.8 and 7.4. As seen, the observed zeroth order rate constants depend (i) for constant (excess) concentration of H_2O_2 linearly on excess concentration of MbFe(III) (**Figure 9A**,**B**) and (ii) for constant (excess) concentration of MbFe(III) linearly on excess concentration of H_2O_2 (**Figure 9C**,**D**). From the slopes of the linear fits in **Figure 9A**−**D**, values of k_8 were estimated by use of eq 17, and the kinetic analysis was validated, since quite similar values were obtained at pH 5.8 from data in **Figure 9A**,**C** (213 ± 9 and 178 ± 17 M^{-1} s^{-1}) and at pH 7.4 from data in **Figure 9B**,**D** (138 ± 5 and 204 ± 4 M^{-1} s^{-1}), respectively. The final common rate constants of the reaction between H_2O_2 and MbFe(III) at pH 5.8 and 7.4 are included in **Table 1**, and notably, the activation of myoglobin by hydrogen peroxide is rather insensitive to pH as k_8 determined at pH 5.8 is not significantly different from k_8 determined at pH 7.4. A common value for the reaction between MbFe(III) and H_2O_2 is estimated to have the value 183 ± 20 M^{-1} s^{-1}.

Lower limits of the rate constants of the reaction between •MbFe(IV)═O and ABTS, k_9, at pH 5.8 and 7.4 were obtained from eq 11, assuming that less than 1% of the myoglobin is present as •MbFe(IV)═O during steady state conditions and using the lowest concentrations of H_2O_2 and MbFe(III) included in this study. Using the common pH-independent value for k_8, a lower limit of 6×10^5 M^{-1} s^{-1} for k_9 was estimated.

Figure 10 shows the results obtained with the assay for determining the catalytic activity of peroxidases by measuring the rate of ABTS oxidation in the presence of H_2O_2 and MbFe(III). The two curves, obtained by smoothed connection of the data points, clearly illustrates a pH-induced difference in the peroxidase activity of myoglobin when the protein is dissolved at pH 7.4 or 5.8.

DISCUSSION

The physiological function of myoglobin is normally considered to be the reversible oxygen storage in the muscles:

$$MbFe(III)O_2 \rightarrow MbFe(II) + O_2 \quad (18)$$

The heme group of myoglobin is identical to the heme group of peroxidases, and because it became evident that myoglobin knockout mice can survive, it has been speculated that myoglobin may have another principal function in mammalians than oxygen storage (*18*). A possible function is the oxidation of nitric oxide:

$$MbFe(II)O_2 + NO \rightarrow MbFe(III) + NO_3^- \quad (19)$$

and it has been suggested that myoglobin rather should be classified as an enzyme (*19*). Besides the oxygenation reaction of eq 19, myoglobin may also enter a peroxidase cycle as shown in **Scheme 1**. The activation of myoglobin in the form of MbFe(III) is possible through the reaction with H_2O_2 or with a lipid hydroperoxide (*20*, *21*). In contrast to H_2O_2 and small organic peroxides, for which the activation is known to proceed through both one and two electron transfer, the reaction stoichiometry for activation by lipid hydroperoxide is still uncertain and should be investigated further. The two hypervalent forms of myoglobin, •MbFe(IV)═O and MbFe(IV)═O, are analogues to the compound I and compound II of the peroxidases, respectively.

Myoglobin and hemoglobin react slower with various substrates than a peroxidase, but under certain conditions, the prooxidative activity of the heme pigments could increase, as has been shown for hemoglobin under acidic conditions (*22*). Peroxidase activity has been suggested to be involved in initiation of lipid oxidation in fish products (*23*). Low pH conditions also occur in meat products, and pH and enzyme conditions in the digestive tract could also enhance pseudoperoxidase activity and in effect initiate radical processes. Other

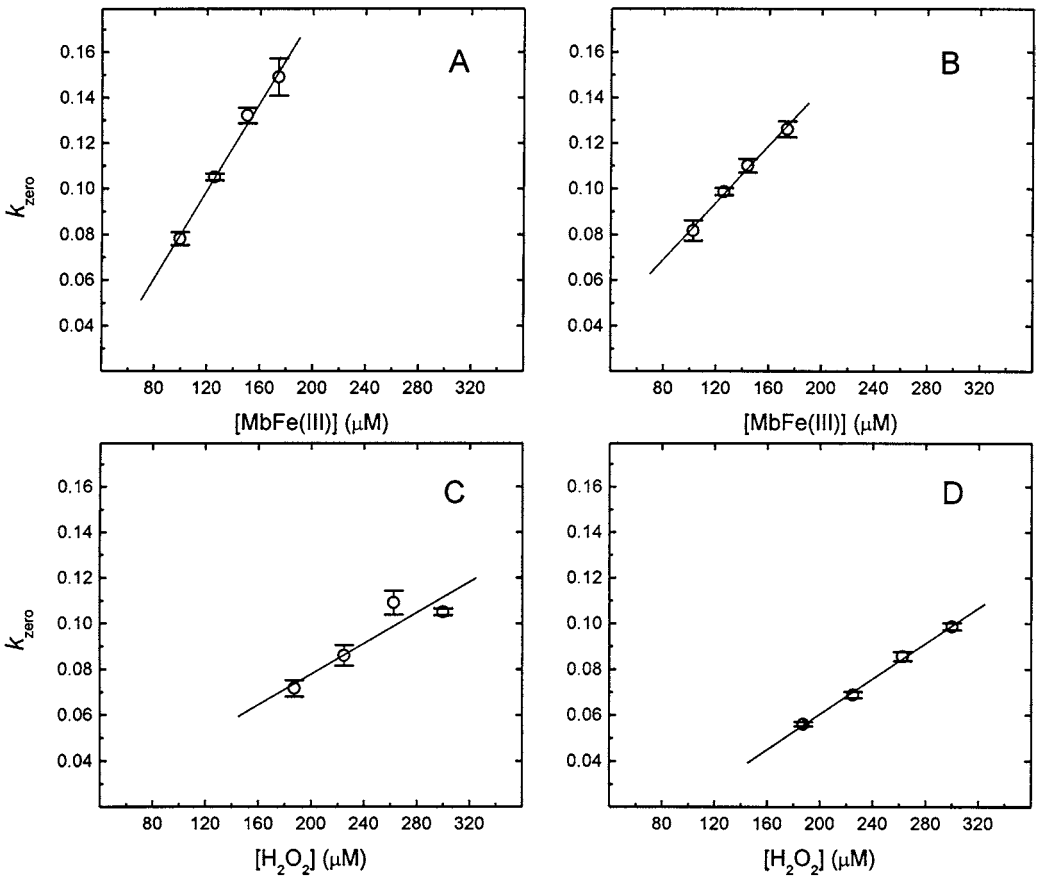

Figure 9. Dependence of the slopes of the zero-order reaction profiles (cf. **Figure 8**) for the reaction at 25.0 °C between ABTS and •MbFe(IV)═O as a function of the initial concentration of H_2O_2 or MbFe(III) at pH 5.74 or pH 7.40 at ionic strength 0.16 (NaCl). (**A**) Prior to exposure to 5.6 μM ABTS at pH 5.74, •MbFe(IV)═O was generated by reaction of varied concentrations of MbFe(III) and 300 μM H_2O_2 for 15 ms. (**B**) Prior to exposure to 5.6 μM ABTS at pH 7.40, •MbFe(IV)═O was generated by reaction of varied concentrations of MbFe(III) and 300 μM H_2O_2 for 30 ms. (**C**) Prior to exposure to 5.6 μM ABTS at pH 5.74, •MbFe(IV)═O was generated by reaction of varied concentrations of H_2O_2 and 126 μM MbFe(III) for 15 ms. (**D**) Prior to exposure to 5.6 μM ABTS at pH 7.40, •MbFe(IV)═O was generated by reaction of varied concentrations of H_2O_2 and 126 μM MbFe(III) for 30 ms.

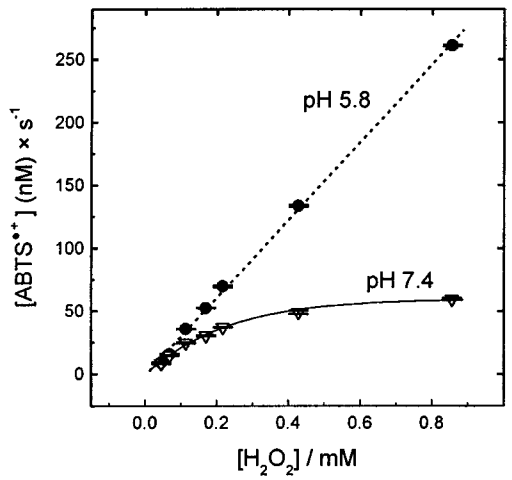

Figure 10. Rate of formation of $ABTS^{\bullet+}$ as a function of [H_2O_2] at 25.0 °C in reaction mixtures of 0.50 μM MbFe(III), 1.0 mM ABTS, and 0.025–0.850 mM H_2O_2 in 50 mM aqueous MES or phosphate buffer.

conditions that might promote peroxidase activity are the proteolysis degrading myoglobin to micromyoglobins (*24*), the treatment of meat in order to enhance iron bioavailability (*25*), or the denaturation by salt, acid, or heat during meat processing.

To quantify such effects and to identify rate-determining steps in the catalytic cycle, the reactivity toward the substrate ABTS was studied using stopped flow absorption spectroscopy. In the

Scheme 1. Peroxidase Cycle of Myoglobin; HA Is a Substrate

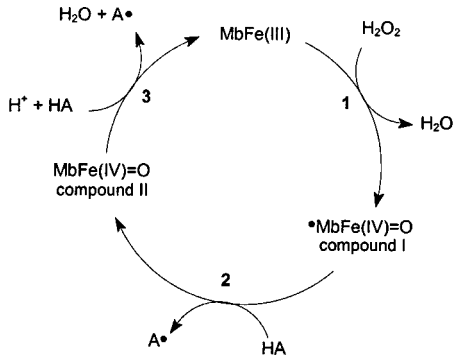

present investigation, only unmodified myoglobin was studied but the results emerge with a clear picture, which clarifies the mechanism behind the effect of decreasing pH. The activation of MbFe(III) to yield •MbFe(IV)═O the analogue of compound I in reaction 1 of **Scheme 1** is slow and independent of pH. The subsequent reaction (reaction 2 of **Scheme 1**) of •MbFe(IV)═O is fast, and only a lower limit for the rate constant could be determined. For unmodified myoglobin, reaction 1 thus becomes rate determining for the activity of compound I.

The catalytic activity of myoglobin is known to increase with decreasing pH. This effect can be assigned to reaction 3 of **Scheme 1**, the oxidation of the substrate by MbFe(IV)═O. This reaction was shown to be of second-order both at high pH and

low pH. Protonization of MbFe(IV)═O yields a more reactive form, and the pK_c value of 5.22 seems to indicate that an imidazole is becoming protonated, which could result in better access to the iron center due to opening of the hydrogen-bonding structure. This better access to the iron center at pH 5.8 where the protonated form of MbFe(IV)═O is more dominating than at pH 7.4 is thus reflected by a significantly lower enthalpy of activation, somewhat counteracted by a negative entropy of activation. This shift from a high value of $\Delta H^{\#}$ and a positive value of $\Delta S^{\#}$ of the reaction at physiological pH (indicating an outersphere mechanism) to a low value of $\Delta H^{\#}$ and the negative value of $\Delta S^{\#}$ for the reaction at pH 5.8 suggests that the protonated form of MbFe(IV)═O reacts through an innersphere mechanism where electrostatic binding of the ABTS anion to MbFe(IV)═O facilitates electron transfer with a substantial degree of binding of the substrate to the compound II analogue.

The reaction mechanisms discussed above for the three steps of the peroxidase cycle are in accordance with the results obtained with the classical peroxidase assay (see **Figure 10**) normally used to investigate steady state kinetics of enzyme activity. At the higher pH, saturation kinetics for the full peroxidase cycle is seen (**Figure 10**) corresponding to an accumulation of compound II following the activation by H_2O_2 and with the subsequent electron transfer step being rather slow. In contrast at low pH, where the electron transfer of reaction 3 in **Scheme 1** is faster, the activation step is becoming rate determining at all H_2O_2 concentrations, and the rate of the overall reaction cycle appears to be in first-order in [H_2O_2]. Such a shift from a simple first-order reaction to saturation kinetics has also been noted for the activation of myoglobin by hydrogen peroxide when the cosubstrate is changed from the more easily oxidized substrate *p*-cresol to tyrosine or tyramine at a constant pH of 6.0 (*3*). The change in mechanism with the change of substrate was also explained by a change in rate-determining step from reaction 1 to reaction 3 of **Scheme 1**. Similarly, when comparing native myoglobin with the myoglobin mutants H64S, H64A, H64L, and H64D, Matsui et al. (*2*) observed a shift from a saturation curve at pH 7.0 (for native myoglobin) to a linear dependency on [H_2O_2] (for the mutants) when measuring the rate of $ABTS^{\bullet+}$ formation after activation of the different myoglobins with hydrogen peroxide. In addition, for the H64D mutant, they found a clear enhanced peroxidase activity since the slope of the linear dependency on [H_2O_2] increased by a factor of ~200 relative to the other myoglobin mutants, reflecting a faster activation (reaction 1 of **Scheme 1**) of the H64D myoglobin.

Our current research effort is concentrated on using the mechanistic assay developed to test various myoglobin derivatives of relevance to meat products for their peroxidase activity and to explain whether the rate-determining step in some instances is changed from reaction 1 to reaction 3 of **Scheme 1** and/or if the rate of the activation reaction (reaction 1 of **Scheme 1**) is increased. The fact that ABTS is oxidized much more rapidly by MbFe(IV)═O than most other substrates investigated (*9*, *26*) makes this substrate more indicative of such changes.

ACKNOWLEDGMENT

Kirsten Sjøstrøm is thanked for excellent technical assistance.

LITERATURE CITED

(1) Sinclair, R.; Hallam, S.; Chen, M.; Chance, B.; Powers, L. Active site structure in cytochrome *c* Peroxidase and myoglobin mutants: Effects of altered hydrogen bonding to the proximal histidine. *Biochemistry* **1996**, *35*, 15120−15128.

(2) Matsui, T.; Ozaki, S.-I.; Watnabe, Y. Formation and catalytic roles of compound 1 in the hydrogen peroxide-dependent oxidations by His64 myoglobin mutants. *J. Am. Chem. Soc.* **1999**, *121*, 9952−9957.

(3) Monzani, E.; Alzuet, G.; Casella, L.; Radaelli, C.; Bassani, C.; Sanangelantoni, A. M.; Gulotti, M.; De Gioia, L.; Santagostini, L.; Chillemi, F. Properties and reactivity of myoglobin with chemically modified protohemin complexes. *Biochemistry* **2000**, *39*, 9571−9582.

(4) Dunford, H. B. *Heme Peroxidases*; John Wiley & Sons: New York, 1999; 507 pp.

(5) Kelman, D. J.; DeGray, J. A.; Mason, R. P. Reaction of myoglobin with hydrogenperoxide forms a peroxyl radical which oxidizes substrates. *J. Biol. Chem.* **1994**, *269*, 7458−7463.

(6) Mikkelsen, A.; Skibsted, L. H. Acid-catalyzed reduction of ferrylmyoglobin: Product distrubution and kinetics of autoreduction and reduction by NADH *Z. Lebensm.-Unters. Forsch.* **1995**, *179*, 1414−1419.

(7) Jørgensen, L. V.; Andersen, H. J.; Skibsted, L. H. Kinetics and reduction of hypervalent iron in myoglobin by crocin in aqueous solution. *Free Radical Res.* **1997**, *27*, 73−87.

(8) Carlsen, C. U.; Kröger-Ohlsen, M. V.; Bellio, R.; Skibsted, L. H. Protein binding in deactivation of ferrylmyoglobin by chlorogenate and ascorbate. *J. Agric. Food Chem.* **2000**, *48*, 204−212.

(9) Kröger-Ohlsen, M. V.; Skibsted, L. H. Deactivation of hypervalent meat pigments. Kinetics of reduction of ferrylmyoglobin by nitrite and iodide. *Food Chem.* **2000**, *70*, 209−214.

(10) Baron, C. P.; Skibsted, L. H.; Andersen, H. J. Prooxidative activity of myoglobin species in linoleic acid emulsions. *J. Agric. Food Chem.* **1997**, *45*, 1704−1710.

(11) Lardinois, O. M.; Ortiz de Montellano, P. R. H_2O_2-mediated cross-linking between lactoperoxidase and myoglobin. *J. Biol. Chem.* **2001**, *276*, 23186−23191.

(12) Andersen, H. J.; Skibsted, L. H. Kinetics and mechanism of thermal oxidation and photooxidation of nitrosylmyoglobin in aqueous solution. *J. Agric. Food Chem.* **1992**, *40*, 1741−1750.

(13) Whitburn, K. D.; Sheih, J. J.; Sellers, R. M.; Hoffmann, M. Z. Redox transformation in ferrimyoglobin induced by radiation-genereated free radicals in aqueous solution. *J. Biol. Chem.* **1982**, *257*, 1860−1869.

(14) Miller, N. J.; Rice-Evans, C.; Davies, M. J.; Gopinathan, V.; Milner, A. A novel method for measuring antioxidant scapacity and its application to monitoring the antioxidant status in premature neonates. *Clin. Sci.* **1993**, *84*, 407−412.

(15) Nelson, D. P.; Kiesow, L. A. Enthalpy of decomposition of hydrogen peroxide at 25 °C (with molar extinction coefficients of H_2O_2 solutions in the UV). *Anal. Biochem.* **1972**, *49*, 474−478.

(16) Childs, R. E.; Beardsley, W. G. The Steady-State Kinetics of Peroxidases with 2.2′-Azino-di-(3-ethyl-benzthiazoline-6-sulphonic acid) as Chromogen. *Biochem. J.* **1975**, *145*, 93−103.

(17) Re, R.; Pellegrini, N.; Proteggente, A.; Pannala, A.; Yang, M.; Rice-Evans, C. Antioxidant activity applying an improved ABTS radical cation decolorization assay. *Free Radical Biol. Med.* **1999**, *26*, 1232−1237.

(18) Flogel, U.; Merx, M. W.; Godecke, A.; Decking, U. K. M.; Shrader, J. Myoglobin: A scavenger of bioactive NO. *Proc. Natl. Acad. Sci. U.S.A.* **2001**, *98*, 735.

(19) Frauenfelder, H.; McMahon, B. H.; Austin, R. H.; Chu, K.; Groves, J. T. The role of structure, energy langscape, dynamics, and allostery in the enzyme function of myoglobin. *Proc. Natl. Acad. Sci. U.S.A.* **2001**, *98*, 2370.

(20) Egawa, T.; Shimada, H.; Ishimura, Y. Formation of compound I in the reaction of native myoglobins with hydrogen peroxide. *J. Biol. Chem.* **2000**, *45*, 34858−34866.

(21) Reeder, B. J.; Wilson, M. T. The effects of pH on the mechanism of hydrogen peroxide and lipid hydroperoxide consumption by myoglobin: A role for the protonated ferryl species. *Free Radical Biol. Med.* **2001**, *30*, 1311−1318.

(22) Kristinsson, H. G. Acid-induced unfolding of flounder hemoglobin: Evidence for a molten globular state with enhanced prooxidative activity. *J. Agric. Food Chem.* **2002**, *50*, 7669−7676.
(23) Richards, M. P.; Hultin, H. O. Contribution of blood components to lipid oxidation in fish muscle. *J. Agric. Food Chem.* **2002**, *50*, 555−564.
(24) Schwarzinger, S.; Arher, W.; Müller, N. Proteolytic preparation of a heme binding fragment from sperm whale myoglobin: Micro-myoglobin. *Monatsh. Chem.* **2000**, *131*, 409−416.
(25) Bæch, S. B.; Hansen, M.; Bukhave, K.; Eriksen, T. A.; Purslow, P. P.; Søndergaard, I.; Friis, A.; Jensen, M.; Skibsted, L. H.; Højgaard, L.; Sandström, B. The effect of specific protein fractions from pork meat on nonheme-iron absorption in humans. *Am. J. Clin. Nutr.*, submitted for publication.
(26) Hu, M.; Skibsted, L. H. Kinetics of reduction of ferrylmyoglobin by (−)-epigallocatechin gallate and green tea extract. *J. Agric. Food Chem.* **2002**, *50*, 2998−3003.

Received for review January 28, 2003. Revised manuscript received June 23, 2003. Accepted July 17, 2003. This research was supported by the FØTEK program through LMC—Center for Advanced Food Studies and by Norma and Frode Jacobsens Fond and the Danish Bacon and Meat Council.

JF030067G